ELSEVIER

Contents lists available at ScienceDirect

Thin-Walled Structures

journal homepage: http://www.elsevier.com/locate/tws



Full length article

Dent-inert post-buckling behavior of liquid nanofoam-filled tube

Check for updates

Fuming Yang ¹, Mingzhe Li ¹, Weiyi Lu ^{*}

Department of Civil & Environmental Engineering, Michigan State University, East Lansing, MI, 48824, USA

ARTICLE INFO

Keywords:
Thin-walled tube
Liquid nanofoam
Dent imperfection
Energy absorption
Buckling mode
Interface

ABSTRACT

Thin-walled tubes have been widely used in crashworthiness applications such as automotive and aerospace industries. However, inevitable structural imperfections in the tube wall impose adverse effects on the energy absorption performance of the tube. Here, we have employed a fluid-like and highly compressible material, i.e. liquid nanofoam (LN), as a filler to suppress the negative impact of structural imperfection. The mechanical performance of empty tubes and LN-filled tubes (LNFT) with different dent imperfections has been evaluated by quasi-static uniaxial compression tests. Results show that empty tube is susceptible to structural imperfection, as a v-shaped dent with 1.5 mm depth reduces the energy absorption capacity by about 20%. In contrast, the mechanical performance of LNFT is insensitive to the existence and depth of the dent. The enhanced imperfection insensitivity of LNFT is due to the intimate liquid-solid interaction at the LN filler and the tube wall interface, which effectively suppresses the curvature growth of the dent and the localized folding. The findings provide an efficient approach for designing and engineering thin-walled energy absorption devices that are resilient and of high energy absorption capacity.

1. Introduction

Thin-walled tubes have been widely applied as energy absorbers, due to their low cost, lightweight and high specific energy absorption capacity. The energy absorption mechanism of thin-walled tubes is based on the tube wall folding [1-3]. To further improve their energy absorption performance, foam materials are usually employed as fillers in thin-walled tubes [4–6]. The axial compressive behaviors of foam-filled thin-walled tubes have been studied by many researchers [7-11]. Sun et al. [12] explored the effect of topological configurations on the energy absorption performance of foam-filled multi-cell tubes and proposed approaches for crashworthiness topology optimization. Zhang et al. [13] and Fang et al. [14] investigated the effect of density gradient of foam fillers on the performance of thin-walled tubes and demonstrated the energy absorption capacity of graded foam-filled tubes outperformed their uniform counterparts. Many other strategies have also been developed for performance enhancement, including but not limited to foam-filled bitubal structures [15,16], ex-situ ordered cellular structure filled tubes [17], tube-filled syntactic foam [18], and metal/CFRP hybrid structures [19].

Despite the enhanced energy absorption performance of thin-walled tubes and their foam-filled counterparts, during the manufacturing,

transporting and handling processes, structural imperfections are inevitably introduced. It has been demonstrated that the load carrying capacity, the post-buckling strength and the energy absorption capacity of thin-walled tubes are significantly compromised when structural imperfections exist [20–26]. However, there is lack of solution to effectively suppress the negative impact of structural imperfections on the mechanical performance of thin-walled tubes.

Recently, a new type of hybrid thin-walled tubes, namely liquid nanofoam-filled tube (LNFT), has shown significantly improved specific energy absorption capacity compared to empty tube and solid foam-filled tubes [27]. The much-enhanced energy absorption performance of the LNFT is due to the intimate filler-tube wall interaction as well as the liquid infiltration behavior of the liquid nanofoam (LN) filler. The fluid-like and highly compressible LN filler is a promising solution to mitigate the negative effect of structural imperfections on the mechanical properties of thin-walled tubes.

The LN filler is a mixture of hydrophobic nanoporous material and a non-wettable liquid [28–33]. The liquid molecules cannot flow into the nanopores spontaneously due to the capillary effect. When an external pressure is applied and reaches a critical value, i.e. the infiltration pressure ($P_{\rm in}$) of LN, the liquid molecules flow into the nanopores and large amount of energy is absorbed during the nanopore filling process.

E-mail address: wylu@egr.msu.edu (W. Lu).

 $^{^{\}ast}$ Corresponding author.

¹ These authors contributed equally to this work.

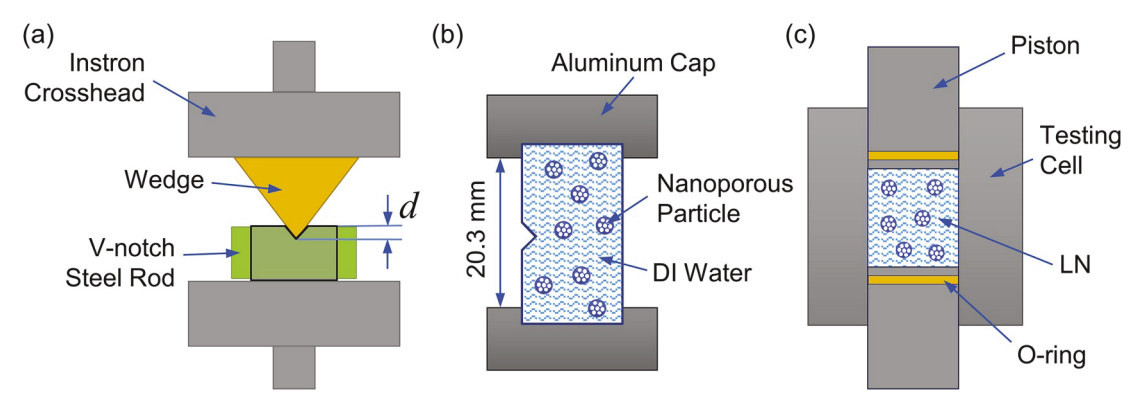


Fig. 1. Defective LNFT sample preparation and experimental setup. (a) Schematic of dent generation with controlled shape and depth, (b) Typical LNFT sample, and (c) Schematic of quasi-static compression tests for the LN filler.

To investigate the effect of the LN filler on thin-walled tubes with structural imperfection, quasi-static uniaxial compression tests have been conducted on LNFTs containing single dent with controlled shape and depth. The mechanical response as well as energy absorption capacity of defective LNFTs have been evaluated to validate the suppression effect of LN filler on dent-induced performance loss.

2. Experimental setup

2.1. Components of LN filler

In this study, the selected nanoporous material was a reversed phase silica gel (Supelco-C8) purchased from Sigma-Aldrich (No. 60759). The Supelco-C8 was hydrophobic as its surface was covered by octylsilane surface groups. The average pore size, specific pore volume, and particle size of the Supelco-C8 were 90 Å, 0.43 $\rm cm^3/g$, and 40–63 μm , respectively. The typical LN filler was composed of 0.5 g Supelco-C8 and 1.0 mL deionized (DI) water. As the Supelco-C8 had hydrophobic surface, a layered structure was formed in the LN sample with one layer of dry Supelco-C8 particles and the other of DI water. If large amount of air had

Strain (mm/mm)

been trapped between hydrophobic Supelco-C8 particles, the performance of the resulted LNFT would be similar to that of empty tube. Therefore, the air content of the LN filler was minimized by a lab-developed pre-compression technique as described in section 2.4.

2.2. Dent with controlled shape and depth

The cylindrical thin-walled tube used in this study was made of stainless steel (SS) 304 and acquired from Microgroup (No. 304F10500 \times 006SL). The outer diameter and the wall thickness of the tube were 12.7 mm and 0.15 mm, respectively. The tube was cut into L=25.4 mm segments for tube sample preparation which will be described in detail in next section. One V-shaped dent was generated at the midspan of each thin-walled tube sample with controlled depth (dent located at 1/2L). As depicted in Fig. 1a, a V-notched solid steel rod template with a diameter of 12.3 mm was firstly inserted into the tube sample. Then, a dent with controlled depth, d, was generated on the tube wall by a wedge attached to an Instron machine (Model 5982). Three dent depths were created on different sample tubes as 0.5 mm, 1.0 mm or 1.5 mm.

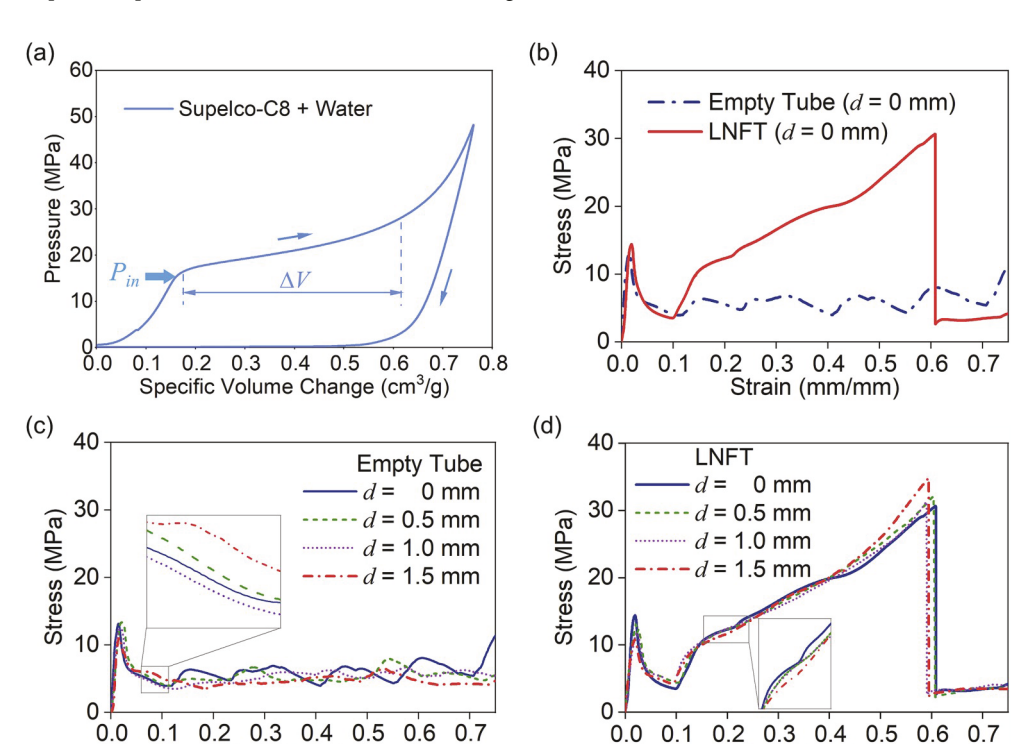


Fig. 2. Quasi-static compression tests on LN filler and LNFTs. (a) Liquid infiltration behavior of LN filler composed of Supelco-C8 and DI water, (b) Continuum behavior of empty tube and LNFT without structural imperfection, (c) Continuum behavior of empty tubes with different dent depths, and (d) Continuum behavior of LNFTs with different dent depths. For comparison purpose, the post-buckling plateau of the purple curve is shifted to match the stress plateaus of other curves. (For interpretation of the reader is reference to the Web version of this article.)

Strain (mm/mm)

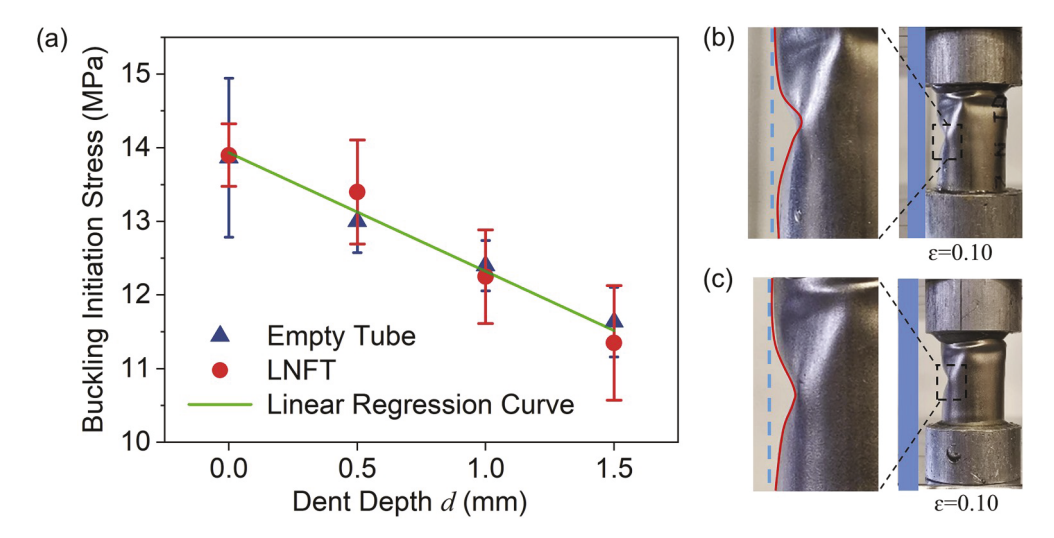


Fig. 3. Dent effect on initial buckling strength and dent-induced bending of empty tube and LNFT. (a) The linearly reduced initial buckling strength with increased dent depth (The error bar is calculated based on three samples), (b–c) Side view of deformed tubes (b) Empty tubes with d = 1.5 mm, and (c) LNFT with d = 1.5 mm.

2.3. Sample preparation of LNFT

Before adding the LN filler into the defective tube, one end of the tube was inserted into an Aluminum cap and sealed by J-B Weld epoxy adhesive (No. 50112). To enhance the sealing quality, thin layer of adhesive was uniformly applied to both the outer surface of the tube and the inner surface of the cap. The adhesive was fully cured at room temperature after 24 h. After that, the LN filler with minimized air content was slowly injected into the tube. Additional DI water was injected into the tube to completely fill the inner space of the tube. As the sealing quality of the epoxy adhesive was sensitive to moisture, a thin layer of grease was carefully placed on the top of the LN filler to eliminate direct contact of water and the adhesive. The tube end was capped and sealed by the same method described above. Once the adhesive layers were applied, the LN-filled tube was vertically clamped on a vice for 24 h to make good alignment of the caps. This was critical to avoid initial bending load on the sample tubes during quasi-static compression tests. The effective tube length of 20.3 mm was measured cap-to-cap distance as shown in Fig. 1b. Empty tubes sealed with two Aluminum caps were used as reference samples.

2.4. Quasi-static compression tests

For the pre-compression and liquid infiltration test of the LN filler, an SS316 testing cell was adopted as sketched in Fig. 1c. The LN filler was sandwiched by two pistons in a cylindrical sleeve. The sealing was accomplished by the O-ring fixed on each piston. The cross-sectional area of the cell, A, was 126 $\,\mathrm{mm}^2$. The difference between pre-compression and liquid infiltration tests was the applied peak force which was 1.85 kN for pre-compression tests and 18 kN for liquid infiltration tests. The loading rate was 2 $\,\mathrm{mm/min}$ for both types of tests. No liquid leakage was observed in all tests.

Uniaxial quasi-static compression tests were conducted on empty tubes and LNFTs. The sample was placed on the Instron platen, and compressed at the loading rate of 2 mm/min. For each dent depth, three samples were tested. No liquid leakage was observed at both sealed ends before tube bursting.

3. Results

Fig. 2a shows typical liquid infiltration behavior of the prepared LN filler. The applied external pressure is calculated as F/A, where F is the applied compression force. The specific volume change is the system volume change normalized by the mass of Supelco-C8 used in the LN

filler. The system volume change is calculated as $V = D \cdot A$, where D is the measured axial displacement of the Instron platen. Under quasistatic loading, the mechanical response of the LN filler is composed of three sections. In the first linear elastic section, the applied external pressure is lower than $P_{\rm in}=17$ MPa, and no liquid molecules can enter the nanopores. In the second plateau section, the liquid molecules overcome the capillary effect and flow into the nanopores with the aid of the applied external pressure. The pressure plateau is defined as the liquid infiltration plateau. The width of the liquid infiltration plateau, ΔV , is about 0.43 cm³/g and matches the total pore volume of Supelco-C8. In the third linear elastic section, all the nanopores are filled by liquid molecules and the LN filler performs as an incompressible liquid. When the applied external pressure is removed, the internal pressure of the LN filler drops quickly to zero. The area enclosed in the hysteretic loading-unloading curve is the specific energy absorption capacity of the LN filler.

Fig. 2b shows the typical stress-strain curves of empty tube and the LNFT. For the empty tube, the initial buckling and post-buckling behaviors are clearly identified. Accordingly, the initial buckling strength (σ_i) is the stress at the ending point of the tube linear elastic response and the post-buckling strength (σ_p) is the average stress of the post-buckling plateau. As illustrated in Fig. 2b, when the strain, ε , is smaller than 0.10, the mechanical response of the LNFT is similar to that of empty tube. This is because of the air trapped in the LN filler. Although precompression technique has been applied to minimize the air content, the hydrophobic nature of Supelco-C8 forms gas-liquid-solid interface around each particle. When ε is in between 0.10 and 0.15, the air effect is eliminated by the tube deformation and then the LNFT performance is dominated by the liquid infiltration behavior of the LN filler. At $\varepsilon = 0.15$, the liquid infiltration is activated at an engineering stress of 11 MPa, which seems lower than the characterized P_{in} of the LN filler. This is due to the lateral expansion of the LNFT, which makes the engineering stress is smaller than the true stress value. When $0.15 = \varepsilon \le 0.60$, a stress plateau with smallest slope in Fig. 2b is observed while the slope of the plateau is larger than that of the infiltration plateau in Fig. 2a. This is attributed to the increased cross-sectional area of the LNFT as well. The plateau width, equivalent to a strain of 0.46, is determined by the total pore volume of Supelco-C8 in the LN filler. At $\varepsilon = 0.61$, the hoop stress developed in the tube wall reaches the failure strength of SS 304 and the LNFT bursts, followed by leakage of the LN filler. The mechanically failed LNFT deforms as an empty tube with vertical dent and has reduced post-buckling strength compared to empty tube, which is dent-free.

The typical continuum behavior of empty tubes and LNFTs with dent is exhibited in Fig. 2c and d. In general, the buckling behavior of tubes

Table 1Snapshots of progressive tube buckling.

ϵ (mm/mm)		0	0.15	0.30	0.45	0.60	
Empty Tube		Reinforcement		Dent-reduced post-	Dent-reduced post-buckling		
	d=0 mm						
	$d=0.5~\mathrm{mm}$		P				
LNFT	$d=1.5~\mathrm{mm}$						
		Trapped air		Dent-suppression by LN filler			
	$d=0~\mathrm{mm}$		Dir				
	d = 0.5 mm		S	13			
	$d=1.5~\mathrm{mm}$						

with dent is similar to that of intact tubes, which is a high-stress initial buckling followed by a post-buckling plateau. With the presence of dent, σ_i of tubes with and without LN filler and σ_p of empty tubes are reduced, while σ_p of LNFTs does not vary too much.

4. Analysis and discussion

4.1. Negative impact of dent on initial buckling strength

As described above, when the axial strain is small (ε < 0.15), the LN filler has no effect on the tube buckling behavior due to the small amount of air trapped at the particle-liquid interface. This is confirmed by Fig. 3a, σ_i of both empty tube and LNFT linearly decreases with increased d. The strength reduction is attributed to the increased size of the dominant structural defect on the tube, i.e. the dent, and the local bending behavior of the defective tube [34]. In previous engineering practice in auto industry, dent geometry and pattern has been designed and applied on thin-walled structures to lower σ_i to approach σ_p for safety purpose [21,35-37]. As the artificial dent is the largest defect on the tube, it acts as the weakest chain and determines σ_i of the resulted tube. In addition, the defective tubes are geometrically asymmetric. The dent-induced localized folding leads to bending of the tubes instead of stabilized buckling, which further reduces σ_i . As revealed in Fig. 3b and c, the dent-induced bending is observed in all defective tubes when $\varepsilon <$ 0.15. Therefore, the presence of the dent negatively affects σ_i of both empty tube and LNFT due to the combined dent size effect and dent-induced local bending.

4.2. Dent effect on post-buckling behavior of empty tube

As shown in Fig. 2c, once the external load reaches σ_i , the load

carrying capacity of all empty tubes drops abruptly by following a same pathway except the defective tube with d=1.5 mm (inset of Fig. 2c). The detailed progressive tube buckling is summarized in Table 1. At $\varepsilon=0.15$, local plastic hinges are fully developed at the top buckling fold of the intact empty tube. Therefore, the tube collapses and temporarily loses all its load carrying capacity till the formation of the 2nd fold. In comparison, for the defective empty tube with d=1.5 mm, the dentinduced bending leads to a larger buckling fold at the bottom half of the tube. The development of the plastic hinges is inhibited by the "central vertical ribbon", which provides the defective tube with additional loading carrying capacity.

With increased axial deformation, the intact empty tube repeats the buckling fold and formation of next fold from one end to the other. As shown in Fig. 2c, the average axial strain of the intact empty tube associated to each buckling fold is around 0.15. After four consecutive diamond buckling folds [3], the tube is solidified. Both the length and the number of buckling fold match well with the theoretical prediction [21,25,26].

With the presence of dent, the post-buckling behavior of the defective tube always initiates at the dent location. As illustrated in Table 1, when d=0.5 mm, the width of the dent in the lateral direction increases. Meanwhile, at $\varepsilon=0.3$, a normal diamond mode wrinkle forms at the top end of the tube. The deformation history of the tube agrees well with the first bump in the post-buckling stress plateau (green curve in Fig. 2c). The peak stress of the bump is close to that of intact empty tube. At this dent depth, the localized buckling fold development is not affected by the dent. As tube buckling progresses (0.35 < ε < 0.5), the tube wall deformation is dominated by the inwards folding of the dent. With increased inwards deformation and dent width, plastic hinges are developed around the dent, which leads to the local collapse of the tube. Therefore, in this dent-dominated region, the stress of the defective tube

is lower and smoother, close to the stress at the nadir of the intact empty tube. At $\varepsilon=0.6$, another normal diamond mode wrinkle forms in the bottom of the tube, which is consistent with the second bump in the post-buckling stress plateau (green curve in Fig. 2c). When the dent depth is relatively small, the defective tube undergoes mixed deformation modes of localized diamond mode folding and dent-dominated collapse. The reduced number of diamond mode folds and the smoother dent-dominated collapse weaken the load carrying capacity of the defective tube.

When d increases to 1.5 mm, not only the width of the dent but also the curvature of the dent increases with larger strain. The whole bottom half of the defective empty tube are dominated by the X-shaped dentinduced plastic hinge (Table 1). The collapse of the plastic hinge leads to a lower and much flatter stress plateau (0.10 < ε < 0.45, red curve in Fig. 2c), which is consistent with previously reported results [38,39]. When the curved and extended dent is in contact with the bottom cap at ε around 0.45 (Table 1), the tube stiffness increases. Thereafter, only one diamond buckling fold is developed in the top half of the defective empty tube, as also indicated by the only bump at $\varepsilon=0.52$ in the red curve in Fig. 2c. With increased dent depth, the dent-induced plastic hinge collapse dominates the post-buckling behavior of the defective tube. Consequently, less buckling folds in diamond mode is fully developed and the load carrying capacity of defective tube is further weakened.

4.3. Dent-inert post-buckling behavior of LNFT

From the stress-strain curves in Fig. 2d, the post-buckling behavior of LNFT is inert to the presence of the dent and the dent depth. Smooth stress plateaus with similar width and stress range are formed in all LNFT tubes with different dent depths. The dent-inert post-buckling behavior of LNFT is attributed to the effect of the LN filler on the dent growth pattern as well as the tube buckling mode.

As shown in Table 1, although the width of the dent grows with increased axial strain of the LNFT with $d=1.5\,\mathrm{mm}$, the curvature of the dent does not change. The pattern of dent growth in LNFT is different from the one in defective empty tube as most of the external loading is carried by the LN filler. Even if plastic hinges were fully developed on the tube wall, the LNFT would not collapse and lose its load carrying capacity. Therefore, the dent-induced local deformation is suppressed by the LN filler.

In addition, the inward diamond buckling fold is prohibited and outward concertina buckling wrinkles are formed along the tube, due to the internally built hydrostatic pressure in the LNFT [27,40]. At larger strain ($\varepsilon > 0.30$), a mixed buckling mode of diamond fold and concertina wrinkle is observed in the LNFT, where the initial buckling fold is formed due to the trapped air in LN filler. The mixed buckling portion of the intact LNFT is much shorter than that of the defective LNFT, which has nearly no effect on the continuum behavior of the LNFTs. Therefore, the buckling behavior of LNFT in the mixed zone is dominated by the concertina buckling triggered by the LN filler. For the rest part of the LNFT, single winkle in defective LNFT or multiple wrinkles in the intact LNFT grow into bulged tubes. The adverse effect of dent is further mitigated by the LN filler, as the localized diamond folding of empty tube is converted into global bulging of the LNFT.

The subtle differences in the stress plateaus in Fig. 2d provide more insight on the suppression effect of the LN filler on dent-induced deformation. As shown in the inset of Fig. 2d, at the onset of the post-buckling plateau (0.15 < ε < 0.30), the stress of LNFTs decreases with increasing dent depth. From the snapshots listed in Table 1, the dent grows in lateral direction and the area around the dent folds inwards. This is due to the relatively weak filler-tube wall interaction, which is not sufficient to fully suppress the dent-induced inwards folding. Previous studies have demonstrated that the filler-tube wall interaction is related to the strength of solid fillers or the infiltration pressure of LN fillers [27,40–42]. Due to the pore size distribution of Supelco-C8, larger

Table 2Energy absorption performance of empty tubes and LNFTs with various dent depths (The error bar is calculated based on three samples).

	d (mm)	Mass (g)	E (J)	SEA (J/g)	E/E_0 (%)
Empty Tube	0	1.29 ± 0.03	8.6 ± 0.2	6.6 ± 0.1	100 ± 2
	0.5	1.29 ± 0.03	8.0 ± 0.4	6.2 ± 0.3	92 ± 3
	1.0	1.29 ± 0.03	7.3 ± 0.3	5.6 ± 0.2	89 ± 2
	1.5	1.29 ± 0.03	7.0 ± 0.6	5.4 ± 0.5	81 ± 5
LNFT	0	3.35 ± 0.05	24.2 ± 0.5	$\textbf{7.2} \pm \textbf{0.2}$	100 ± 4
	0.5	3.30 ± 0.07	23.8 ± 0.6	$\textbf{7.2} \pm \textbf{0.2}$	99 ± 5
	1.0	3.26 ± 0.08	23.6 ± 0.8	7.3 ± 0.3	98 ± 6
	1.5	3.24 ± 0.08	23.5 ± 0.6	$\textbf{7.3} \pm \textbf{0.2}$	98 ± 5

nanopores are firstly triggered for liquid infiltration, which provides a relatively lower $P_{\rm in}$ of 17 MPa. Therefore, the stress of defective LNFTs is adversely affected by the dent. As $\varepsilon > 0.40$, the higher $P_{\rm in}$ associated with smaller nanopores in the LN enhances the filler-tube wall interaction, so that the inwards folding of the dent is fully suppressed. Apparently, no dent-induced collapse is allowed in LNFT. Meanwhile, the tube wall itself becomes more prone to buckle inwards as the folding collapse progresses. The dent-induced plastic deformation of the tube wall leads to an enhanced strain hardening effect [40,43], which results the improved filler-tube wall interaction as well as the load-bearing capacity of the defective LNFT and helps the tube wall to hold higher $P_{\rm in}$ [44] at the end of the post-buckling plateau (0.40 < ε < 0.60 in Fig. 2d). Therefore, the burst stress of LNFT is increased from 30 MPa to 34 MPa as dent depth changes from 0 to 1.5 mm (Fig. 2d).

As an energy absorber, it is vital to evaluate the energy absorption capacity [45,46], *E*, of the empty tubes and LNFTs with various dent depths by using Eq. (1), and their specific energy absorption capacity (energy per unit mass), *SEA*, given by Eq. (2).

$$E = V_0 \int_0^{\varepsilon_b} \sigma d\varepsilon \,\# \tag{1}$$

where V_0 is the effective tube volume.

$$SEA = \frac{E}{m} \# \tag{2}$$

where m is the mass. The results are summarized in Table 2. The energy absorption capacity of the intact empty tube and the LNFT are 8.6 J and 24.2 J, respectively. Fig. 4a depicts the relationship between the retained energy absorption capacity and the dent depth of both empty tubes and LNFTs. For emtpy tubes, by increasing d from 0 mm to 1.5 mm, the retained energy absorption capacity linearly decreases to 82% of the intact empty tube. For LNFTs, the retained energy absorption capacity silightly decreases (<2%) with the presence of dent, which is mainly resulted from the reduced σ_i . Similar trends are also observed in the SEA curves in Fig. 4b. The SEA of empty tubes keeps decreasing with increased dent depth, while the SEA of LNFT slightly increases due to the reduced mass of the whole composite structure. Clearly, the negative impact of the dent on the post-buckling behavior of thin-walled tube is effectively suppressed by the LN filler. With the existence of the LNfiller, hydrostatic pressure is uniformly built up in the LNFTs, which is independent from the compression direction. However, the compression direction may alter the tube wall buckling mode into a bending one. The additinoal LN-filler effectively enhances the bending stiffness of the LNFts and thus enhances the energy dissipation in the bending mode as

To further study the effect of dent location, empty tube and LNFT samples with dent located at 1/4 of the tube length were prepared and evaluated under the same testing conditions. Fig. 5 shows the effect of dent location on the mechanical repsonse of emtpy tubes and LNFTs. For empty tubes, as the dent location changes from 0.5 L to 0.25 L, the post-buckling behavior remains the same except that the stress level is slightly reduced (Fig. 5a). This stress reduction is attributed to the

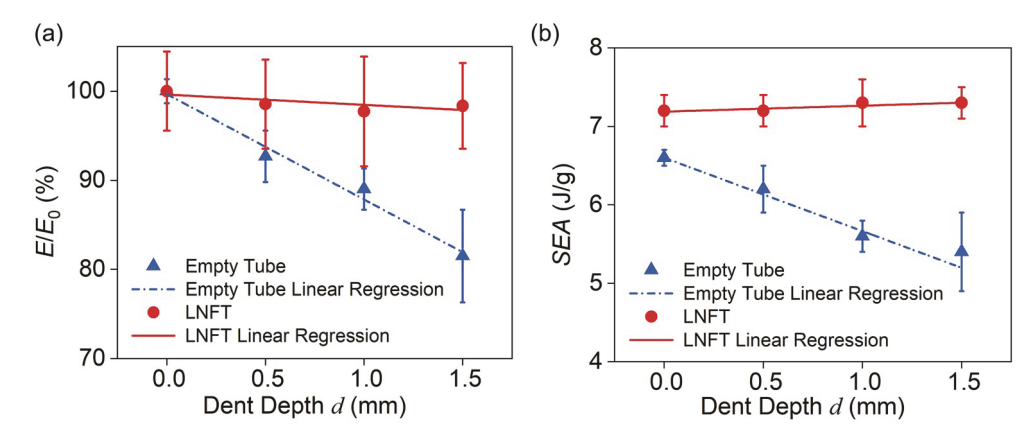


Fig. 4. Dent-suppression effect of the LN filler. (a) The retained energy absorption capacity of defective empty tubes and LNFTs compared to their intact counterparts, and (b) The SEA of empty tubes and LNFTs with various dent depths (The error bar is calculated based on three samples).

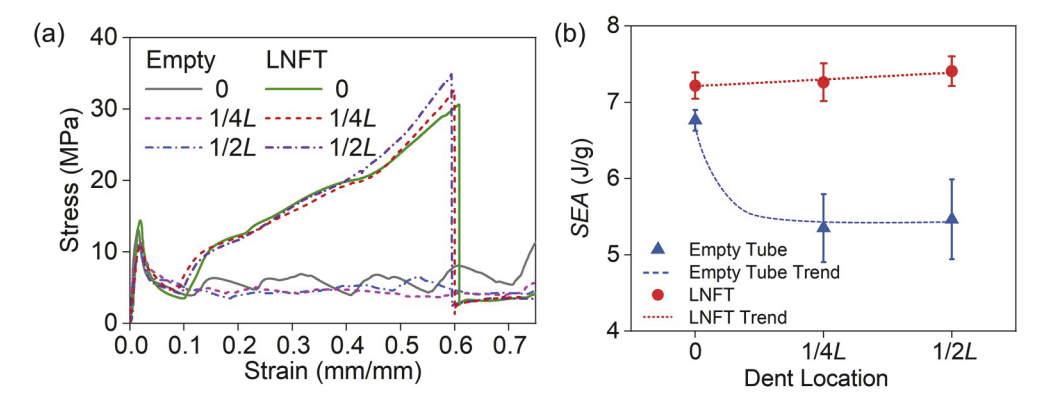


Fig. 5. Effect of dent location on the performance of empty tubes and LNFTs with dent depth d = 1.5 mm. Dent location at 0 means dent-free. (a) Continuum behavior of empty tubes and LNFTs with different dent locations, and (b) The SEA of empty tubes and LNFTs with different dent locations.

asymmetry induced system instability. The mechanical reponse of LNFTs with different dent locations is stable, indicating the dent location effect is negligible. This is further validated by the *SEA* shown in Fig. 5b. The dent-suppression effect of the LN-filler is independent from the dent location.

5. Conclusions

The effect of dent on thin-walled tubes with and without LN filler has been investigated by quasi-static uniaxial compression tests. Based on the comparison of energy absorption performance of thin-walled tubes with and without LN filler, the following conclusions are drawn:

- The empty tube is vulnerable to dent which greatly reduces the initial buckling strength, the post-buckling strength and the energy absorption capacity.
- The reduction in mechanical performance of empty tube is linearly proportional to the dent depth.
- In contrast, the LNFT is inert to dent depth and location, as demonstrated by the preserved energy absorption capacity.
- The underlying mechanism of the dent-inert energy absorption performance of LNFT is the intimate liquid-solid interaction at the LN filler and the tube wall interface, suppressing the curvature growth of the dent and the localized folding.

In short, The LN filler not only increases the energy absorption capacity and SEA of LNFT, but also provides an economical approach to reduce the cost on quality control and handling of thin-walled structures.

Declaration of competing interest

The authors declare that they have no known competing financial interests or personal relationships that could have appeared to influence the work reported in this paper.

CRediT authorship contribution statement

Fuming Yang: Formal analysis, Writing - original draft. **Mingzhe Li:** Methodology, Data curation, Writing - original draft. **Weiyi Lu:** Conceptualization, Data curation, Writing - review & editing, Supervision, Funding acquisition.

Acknowledgements

This research is financially supported by the National Science Foundation grant (No. CBET-1803695) and Michigan State University Startup grant.

References

- T. Wierzbicki, W. Abramowicz, On the crushing mechanics of thin-walled structures, J. Appl. Mech. 50 (1983) 727–734, https://doi.org/10.1115/ 1.3167.327
- [2] M. Langseth, O.S. Hopperstad, A.G. Hanssen, Crash behaviour of thin-walled aluminium members, Thin-Walled Struct. 32 (1998) 127–150, https://doi.org/ 10.1016/S0263-8231(98)00030-5.
- [3] K.R.F. Andrews, G.L. England, E. Ghani, Classification of the axial collapse of cylindrical tubes under quasi-static loading, Int. J. Mech. Sci. 25 (1983) 687–696, https://doi.org/10.1016/0020-7403(83)90076-0.

- [4] J. Fang, G. Sun, N. Qiu, N.H. Kim, Q. Li, On design optimization for structural crashworthiness and its state of the art, Struct. Multidiscip. Optim. 55 (2017) 1091–1119, https://doi.org/10.1007/s00158-016-1579-y.
- [5] A. Baroutaji, M. Sajjia, A.-G. Olabi, On the crashworthiness performance of thin-walled energy absorbers: recent advances and future developments, Thin-Walled Struct. 118 (2017) 137–163, https://doi.org/10.1016/J.TWS.2017.05.018.
- [6] I. Duarte, L. Krstulović-Opara, J. Dias-de-Oliveira, M. Vesenjak, Axial crush performance of polymer-aluminium alloy hybrid foam filled tubes, Thin-Walled Struct. 138 (2019) 124–136, https://doi.org/10.1016/J.TWS.2019.01.040.
- [7] A.R.C. Duarte, B. Ünal, J.F. Mano, R.L. Reis, K.F. Jensen, Microfluidic production of perfluorocarbon-alginate core-shell microparticles for ultrasound therapeutic applications, Langmuir 30 (2014) 12391–12399, https://doi.org/10.1021/ la502822y
- [8] M. Su, H. Wang, H. Hao, Axial and radial compressive properties of aluminaaluminum matrix syntactic foam filled thin-walled tubes, Compos. Struct. 226 (2019) 111197, https://doi.org/10.1016/J.COMPSTRUCT.2019.111197.
- [9] M. Taherishargh, M. Vesenjak, I.V. Belova, L. Krstulović-Opara, G.E. Murch, T. Fiedler, In situ manufacturing and mechanical properties of syntactic foam filled tubes, Mater. Des. 99 (2016) 356–368, https://doi.org/10.1016/J. MATDES 2016 03 027
- [10] E. Linul, D. Lell, N. Movahedi, C. Codrean, T. Fiedler, Compressive properties of zinc syntactic foams at elevated temperatures, Compos. B Eng. 167 (2019) 122–134, https://doi.org/10.1016/J.COMPOSITESB.2018.12.019.
- [11] L. Pan, Y. Yang, M.U. Ahsan, D.D. Luong, N. Gupta, A. Kumar, P.K. Rohatgi, Zn-matrix syntactic foams: effect of heat treatment on microstructure and compressive properties, Mater. Sci. Eng. 731 (2018) 413–422, https://doi.org/10.1016/J. MSEA.2018.06.072.
- [12] G. Sun, T. Liu, X. Huang, G. Zheng, Q. Li, Topological configuration analysis and design for foam filled multi-cell tubes, Eng. Struct. 155 (2018) 235–250, https:// doi.org/10.1016/J.ENGSTRUCT.2017.10.063.
- [13] Z. Yi, H. Si-yuan, L. Jia-gui, Z. Wei, G. Xiao-lu, Y. Jin, Density gradient tailoring of aluminum foam-filled tube, Compos. Struct. 220 (2019) 451–459, https://doi.org/ 10.1016/J.COMPSTRUCT.2019.04.026.
- [14] J. Fang, Y. Gao, X. An, G. Sun, J. Chen, Q. Li, Design of transversely-graded foam and wall thickness structures for crashworthiness criteria, Compos. B Eng. 92 (2016) 338–349, https://doi.org/10.1016/J.COMPOSITESB.2016.02.006.
- [15] G. Sun, Z. Wang, H. Yu, Z. Gong, Q. Li, Experimental and numerical investigation into the crashworthiness of metal-foam-composite hybrid structures, Compos. Struct. 209 (2019) 535–547, https://doi.org/10.1016/J. COMPSTRUCT.2018.10.051.
- [16] Y. Zhang, G. Sun, G. Li, Z. Luo, Q. Li, Optimization of foam-filled bitubal structures for crashworthiness criteria, Mater. Des. 38 (2012) 99–109, https://doi.org/ 10.1016/J.MATDES.2012.01.028.
- [17] H. Wang, M. Su, H. Hao, The quasi-static axial compressive properties and energy absorption behavior of ex-situ ordered aluminum cellular structure filled tubes, Compos. Struct. 239 (2020) 112039, https://doi.org/10.1016/J. COMPSTRUCT.2020.112039.
- [18] N. Movahedi, G.E. Murch, I.V. Belova, T. Fiedler, Manufacturing and compressive properties of tube-filled metal syntactic foams, J. Alloys Compd. 822 (2020) 153465, https://doi.org/10.1016/J.JALLCOM.2019.153465.
- [19] G. Zhu, J. Liao, G. Sun, Q. Li, Comparative study on metal/CFRP hybrid structures under static and dynamic loading, Int. J. Impact Eng. (2020) 103509, https://doi. org/10.1016/J.UIMPENG.2020.103509
- [20] A.G. Mamalis, G.L. Viegelahn, D.E. Manolakos, W. Johnson, Experimental investigation into the axial plastic collapse of steel thin-walled grooved tubes, Int. J. Impact Eng. 4 (1986) 117–126, https://doi.org/10.1016/0734-743X(86)90012-
- [21] T. Ghanbari Ghazijahani, H. Jiao, D. Holloway, Experimental study on damaged cylindrical shells under compression, Thin-Walled Struct. 80 (2014) 13–21, https://doi.org/10.1016/J.TWS.2014.02.029.
- [22] T. Ghanbari Ghazijahani, H. Jiao, D. Holloway, Plastic buckling of dented steel circular tubes under axial compression: an experimental study, Thin-Walled Struct. 92 (2015) 48–54, https://doi.org/10.1016/j.tws.2015.02.018.
- [23] N.S. Marshall, G.N. Nurick, Effect of induced imperfections on the formation of the first lobe of symmetric progressive buckling of thin-walled square tubes, Int. Conf. Struct. Under Shock Impact, SUSI. 32 (1998) 155–168.
- [24] J.C. Amazigo, B. Budiansky, J.C. Amazigo, B. Bidiansky, Asymptotic formulas for the buckling stresses of axially compressed cylinders with localized or random

- axisymmetric imperfections, J. Appl. Mech. 39 (1972) 179–184, https://doi.org/ 10.1115/1.3422608.
- [25] W. Guggenberger, Buckling and postbuckling of imperfect cylindrical shells under external pressure, Thin-Walled Struct. 23 (1995) 351–366, https://doi.org/ 10.1016/0263-8231(95)00022-6.
- [26] A. Khamlichi, M. Bezzazi, A. Limam, Buckling of elastic cylindrical shells considering the effect of localized axisymmetric imperfections, Thin-Walled Struct. 42 (2004) 1035–1047, https://doi.org/10.1016/j.tws.2004.03.008.
- [27] M. Li, J. Li, S. Barbat, R. Baccouche, W. Lu, Enhanced filler-tube wall interaction in liquid nanofoam-filled thin-walled tubes, Compos. Struct. 200 (2018) 120–126, https://doi.org/10.1016/j.compstruct.2018.05.101.
- [28] M. Li, W. Lu, Liquid marble: a novel liquid nanofoam structure for energy absorption, AIP Adv. 7 (2017), 055312, https://doi.org/10.1063/1.4984231
- [29] M. Li, W. Lu, Adaptive liquid flow behavior in 3D nanopores, Phys. Chem. Chem. Phys. 19 (2017) 17167–17172, https://doi.org/10.1039/C7CP02981K.
- [30] Y. Zhang, M. Li, Y. Gao, B. Xu, W. Lu, Compressing liquid nanofoam systems: liquid infiltration or nanopore deformation? Nanoscale 10 (2018) 18444–18450, https:// doi.org/10.1039/c8nr04233k.
- [31] L. Liu, X. Chen, W. Lu, A. Han, Y. Qiao, Infiltration of electrolytes in molecularsized nanopores, Phys. Rev. Lett. 102 (2009) 184501, https://doi.org/10.1103/ PhysRevLett.102.184501.
- [32] F.B. Surani, Y. Qiao, Infiltration and defiltration of an electrolyte solution in nanopores, J. Appl. Phys. 100 (2006) 1–5, https://doi.org/10.1063/1.2222042
- [33] A. Han, W. Lu, T. Kim, X. Chen, Y. Qiao, Influence of anions on liquid infiltration and defiltration in a zeolite y, Phys. Rev. E - Stat. Nonlinear Soft Matter Phys. 78 (2008) 3–6, https://doi.org/10.1103/PhysRevE.78.031408.
- [34] B. Prabu, A.V. Raviprakash, A. Venkatraman, Parametric study on buckling behaviour of dented short carbon steel cylindrical shell subjected to uniform axial compression, Thin-Walled Struct. 48 (2010) 639–649, https://doi.org/10.1016/J. TWS.2010.02.009.
- [35] M. Ferdynus, M. Kotelko, M. Urbaniak, Crashworthiness performance of thin-walled prismatic tubes with corner dents under axial impact numerical and experimental study, Thin-Walled Struct. 144 (2019) 106239, https://doi.org/10.1016/j.tws.2019.106239.
- [36] C.C. Zhao, J. Niu, Q. Zhang, C.C. Zhao, J. Xie, Buckling behavior of a thin-walled cylinder shell with the cutout imperfections, Mech. Adv. Mater. Struct. (2018) 1–7, https://doi.org/10.1080/15376494.2018.1444225, 0.
- [37] T. Ghanbari Ghazijahani, H. Jiao, D. Holloway, Experiments on dented cylindrical shells under peripheral pressure, Thin-Walled Struct. 84 (2014) 50–58, https://doi. org/10.1016/j.tws.2014.05.012.
- [38] K. Yang, S. Xu, S. Zhou, J. Shen, Y.M. Xie, Design of dimpled tubular structures for energy absorption, Thin-Walled Struct. 112 (2017) 31–40, https://doi.org/ 10.1016/J.TWS.2016.12.003.
- [39] N.S. Ha, G. Lu, X. Xiang, High energy absorption efficiency of thin-walled conical corrugation tubes mimicking coconut tree configuration, Int. J. Mech. Sci. 148 (2018) 409–421, https://doi.org/10.1016/J.IJMECSCI.2018.08.041.
- [40] Y. Liu, T.A. Schaedler, A.J. Jacobsen, W. Lu, Y. Qiao, X. Chen, Quasi-static crush behavior of hollow microtruss filled with NMF liquid, Compos. Struct. 115 (2014) 29–40, https://doi.org/10.1016/j.compstruct.2014.03.047.
- [41] Y. Liu, T.A. Schaedler, A.J. Jacobsen, X. Chen, Quasi-static energy absorption of hollow microlattice structures, Compos. B Eng. 67 (2014) 39–49, https://doi.org/ 10.1016/j.compositesb.2014.06.024.
- [42] I. Duarte, M. Vesenjak, L. Krstulović-Opara, Z. Ren, Compressive performance evaluation of APM (Advanced Pore Morphology) foam filled tubes, Compos. Struct. 134 (2015) 409–420, https://doi.org/10.1016/j.compstruct.2015.08.097.
 [43] A.K. De, J.G. Speer, D.K. Matlock, D.C. Murdock, M.C. Mataya, R.J. Comstock,
- [43] A.K. De, J.G. Speer, D.K. Matlock, D.C. Murdock, M.C. Mataya, R.J. Comstock, Deformation-induced phase transformation and strain hardening in type 304 austenitic stainless steel, Metall. Mater. Trans. 37 (2006) 1875–1886, https://doi. org/10.1007/s11661-006-0130-y.
- [44] D. Camilleri, D. Mackenzie, R. Hamilton, Material strain hardening in pressure vessel design by analysis, Proc. Inst. Mech. Eng. Part E J. Process Mech. Eng. 221 (2007) 89–100, https://doi.org/10.1243/0954408JPME107.
- [45] G. Sun, H. Yu, Z. Wang, Z. Xiao, Q. Li, Energy absorption mechanics and design optimization of CFRP/aluminium hybrid structures for transverse loading, Int. J. Mech. Sci. 150 (2019) 767–783, https://doi.org/10.1016/J. IJMECSCI.2018.10.043.
- [46] W. Zhang, S. Yin, T.X. Yu, J. Xu, Crushing resistance and energy absorption of pomelo peel inspired hierarchical honeycomb, Int. J. Impact Eng. 125 (2019) 163–172, https://doi.org/10.1016/J.IJIMPENG.2018.11.014.